Journal for Multiscale Computational Engineering, 10 (6): 527–549 (2012)

EVALUATION OF GENERALIZED CONTINUUM SUBSTITUTION MODELS FOR HETEROGENEOUS MATERIALS

Duy Khanh Trinh,[1] Ralf Jänicke,[2] Nicolas Auffray,[3] Stefan Diebels,[4] & Samuel Forest[1,*]

[1]*MINES ParisTech, Centre des matériaux, CNRS UMR 7633, BP 87, F–91003 Evry Cedex, France*

[2]*Ruhr-Universität Bochum, Institut für Mechanik-Kontinuumsmechanik, IA 3/28, Universitätsstr. 150, D–44780 Bochum, Germany*

[3]*Laboratoire Modélisation et Simulation Multi-échelles (MSME), UMR 8208 CNRS, Université Paris-Est Marne-la-Vallée, 5 Bd Descartes, D–77454 Marne-la-Vallée, France*

[4]*Universität des Saarlandes, Lehrstuhl fuer Technische Mechanik, Postfach 15 11 50, D–66041 Saarbrücken, Germany*

[*] Address all correspondence to Samuel Forest, E-mail: samuel.forest@ensmp.fr

Several extensions of standard homogenization methods for composite materials have been proposed in the literature that rely on the use of polynomial boundary conditions enhancing the classical affine conditions on the unit cell. Depending on the choice of the polynomial, overall Cosserat, second gradient, or micromorphic homogeneous substitution media are obtained. They can be used to compute the response of the composite when the characteristic length associated with the variation of the applied loading conditions becomes of the order of the size of the material inhomogeneities. A significant difference between the available methods is the nature of the fluctuation field added to the polynomial expansion of the displacement field in the unit cell, which results in different definitions of the overall stress and strain measures and higher order elastic moduli. The overall higher order elastic moduli obtained from some of these methods are compared in the present contribution in the case of a specific periodic two-phase composite material. The performance of the obtained overall substitution media is evaluated for a chosen boundary value problem at the macroscopic scale for which a reference finite element solution is available. Several unsatisfactory features of the available theories are pointed out, even though some model predictions turn out to be highly relevant. Improvement of the prediction can be obtained by a precise estimation of the fluctuation at the boundary of the unit cell.

KEY WORDS: *higher order homogenization, composite materials, Cosserat, second gradient, micromorphic theory, polynomial boundary conditions, representative volume element, finite element*

1. INTRODUCTION

Standard homogenization methods for composite materials are known to fail when the size of the constituents of heterogeneous materials is not sufficiently small with respect to the size of the structure or the characteristic size of variation of the macroscopic mechanical fields. Heuristic enhancements of the homogenization procedures have been proposed to overcome this limitation, based on correctors from multiscale asymptotic expansion by Boutin (1996), or on polynomial expansion of the microscopic field in Forest (1998), Gologanu et al. (1997), and Ostoja-Starzewski et al. (1999). The multiscale asymptotic expansion approach has the merit to deliver a systematic method to compute new correctors, even though there is no theoretical certitude that the use of the correctors will greatly improve the

1543–1649/12/$35.00

prediction. This is due to the fact that boundary layers effects play a significant role in the analysis of structures containing a periodic distribution of heterogeneities with non-negligible size. Furthermore, the methodology can hardly be extended to non-linear material behavior because of the complexity of the required incremental asymptotic analysis. In contrast, the use of polynomial boundary conditions to be prescribed on a representative volume element in order to determine higher order effective properties can be applied to non–linear material response as done in Feyel (2003), Forest (1999), Geers et al. (2001), Kouznetsova et al. (2004b), and Trovalusci and Masiani (2003). However, the polynomial expansion approach to higher order homogenization remains heuristic and no fully satisfying procedure seems to emerge from the previous attempts (Forest and Trinh, 2011).

First, the polynomial approach relies on the choice of a well-suited higher order continuum theory at the macro-level, as a homogeneous substitution medium. Multiscale asymptotic methods generally lead to the definition of an overall second gradient model (Dell'Isola et al., 1998; Triantafyllidis and Bardenhagen, 1996). The second gradient model has also been retained in the polynomial approach by Bacigalupo and Gambarotta (2010), Kaczmarczyk et al. (2008), Kouznetsova et al. (2004b), and Mühlich et al. (2009). However, the homogeneous substitution medium can also include additional degrees of freedom,such as micro-rotations in the Cosserat model or full microdeformation according to the micromorphic approach. This is the three-dimensional counterpart of the choice of Bernoulli and Timoshenko models for composite beams. These additional macroscopic kinematic quantities must be defined as well-suited averages over the heterogeneous material unit cell. The Cosserat and closely related couple-stress models were used as homogeneous substitution media for various composite materials by Bigoni and Drugan (2007); De Bellis and Addessi (2010); Forest and Sab (1998); Larsson and Diebels (2007); Masiani and Trovalusci (1996); Trovalusci and Masiani (2003). In particular, foams or lattice structures have been modeled by means of such Cosserat or micromorphic models Dillard et al. (2006); Ebinger et al. (2005); Tekoglu and Onck (2008). There is however no systematic rule to select the proper generalized continuum theory at the macro-level when considering the polynomial expansion method. The micromorphic model put forward in Jänicke et al. (2009) has the advantage that it encompasses the Cosserat as well as the second gradient approach as limited cases corresponding to specific values of constitutive properties.

Second, different ways of applying polynomial non-homogeneous boundary conditions to the material's unit cell have been explored in the literature, as extensions of the usual affine conditions of standard homogenization. Quadratic or higher order polynomial conditions can be applied directly at the boundary of the representative volume element, as done in Gologanu et al. (1997) and Jänicke et al. (2009). In that case, however, when considering quadratic conditions for instance, the average second gradient cannot be strictly controlled (Forest and Trinh, 2011). Also, Dirichlet conditions are known to lead to too stiff overall moduli. The introduction of a fluctuation displacement field is therefore necessary. The fluctuation was chosen periodic in Forest and Sab (1998) and Kouznetsova et al. (2004b), as in standard homogenization of periodic composites, but this choice is not entirely satisfactory, as discussed in Bacigalupo and Gambarotta (2010), Forest and Trinh (2011), Kaczmarczyk et al. (2008), and Yuan et al. (2008), where alternative conditions of the fluctuation fields are also proposed.

Finally, homogenization methods rely on the definition of a representative volume element (RVE) for the composite material. The definition of a RVE for the higher order homogenization turns out to be a difficult task in contrast to classical homogenization for which clear procedures exists for both periodic and random heterogeneous materials Kanit et al. (2003). For periodic medium, the question of RVE size for the determination of generalized continuum properties has hardly been undertaken. It was shown by Kouznetsova et al. (2004b) that the effective second gradient moduli scale with a power law of the size of volume element (i.e., of the number of unit cells in the volume element). In contrast, it seems that a satisfactory homogenization procedure should produce effective moduli that do not depend on the size of the volume element as soon as the RVE size is reached (i.e., the unit cell size for a periodic media). Such a procedure has been proposed in Forest and Trinh (2011) and will be used in the present contribution. Also the higher order effective properties should not depend on the specific choice of the unit cell for a periodic medium, as in the classical case. This required property is not met by the available higher order computational homogenization techniques.

The present work addresses several questions still unsolved in the problem of generalized continuum homogenization. The objective is to compare the values and the performance of the overall higher order elastic properties derived from several of the available mentioned higher order homogenization techniques. This is done in the special case of a

highly contrasted elastic two-phase periodic material with a given unit cell geometry. The overall moduli of Cosserat, second gradient, and micromorphic substitution media will be determined for different hypotheses regarding the fluctuation displacement field. The performance of the obtained substitution media is evaluated by considering a specific boundary value problem on the heterogeneous material for which classical homogenization will be shown to fail.

Some available micro-macroscale transition rules for higher order continua are recalled in Section 2. The polynomial boundary conditions are explicited in Section 3 where the question of RVE size for higher order homogenization is also addressed. The overall higher order elastic properties are identified in Section 4 for three different fluctuation conditions in the case of a given composite microstructure. In the final section, a reference computation is performed on the fully discretized heterogeneous structure under specific loading conditions. This reference is compared to the estimations of the overall Cosserat, second gradient, and micromorphic substitution media.

The analysis is restricted to linear elasticity within the small strain framework. All deformed states presented in the figures are magnified for better illustration.

In this work, zeroth-, first-, second- and third-order tensors are denoted by $a, \underline{\boldsymbol{a}}, \underline{\underline{\boldsymbol{a}}}, \underline{\underline{\underline{\boldsymbol{a}}}}$, respectively. The simple, double and triple contractions are written ".", ":", and ":", respectively. In index form with respect to an orthonormal Cartesian basis, these notations correspond to

$$\underline{\boldsymbol{a}} . \underline{\boldsymbol{b}} = a_i b_j, \quad \underline{\underline{\boldsymbol{a}}} : \underline{\boldsymbol{b}} = a_{ij} b_{ij}, \quad \underline{\underline{\underline{\boldsymbol{a}}}} \vdots \underline{\underline{\boldsymbol{b}}} = a_{ijk} b_{ijk} \tag{1}$$

where repeated indices are summed up. The tensor product is denoted by $\otimes$. For example, the component $(\underline{\underline{\boldsymbol{a}}} \otimes \underline{\boldsymbol{b}})_{ijkl}$ is $a_{ij} b_{kl}$. The ∇ operator is denoted by $\boldsymbol{\nabla}_X$ (resp. $\boldsymbol{\nabla}_x$) when partial derivation is computed with respect to macroscopic (resp. microscopic) coordinates. For example, $\underline{\underline{\boldsymbol{\sigma}}} . \boldsymbol{\nabla}$ is the divergence of the second-order tensor $\underline{\underline{\boldsymbol{\sigma}}}$. The index form of $\underline{\underline{\boldsymbol{\sigma}}} . \boldsymbol{\nabla}$ is $\sigma_{ij,j}$. Similarly, $\underline{\boldsymbol{u}} \otimes \boldsymbol{\nabla}$ means $u_{i,j}$. The sign $:=$ defines the quantity on the left-hand side.

2. DEFINITION OF GENERALIZED EFFECTIVE CONTINUUM

The extended homogenization procedures based on the use of non–homogeneous polynomial loading conditions of the heterogeneous material's unit cell generally rely on the a priori choice of a targeted generalized continuum. The number of independent coefficients in the considered polynomial must increase if the kinematics of the overall generalized continuum is enriched. The most general situation at the macroscopic scale considered in the literature yet is the micromorphic continuum. We first recall the homogenization procedure for micromorphic overall continua according to Forest (2002) and Jänicke et al. (2009). We then show how this general situation reduces to second gradient and Cosserat overall continua as special cases that were independently proposed in Forest and Sab (1998) and Gologanu et al. (1997) respectively.

2.1 Micromorphic Overall Continuum

The micromorphic theory first proposed by Eringen and Suhubi (1964) and Mindlin (1964) introduces microdeformation degrees of freedom represented by the generally non-symmetric second-order tensor field, $\underline{\underline{\boldsymbol{\chi}}}(\underline{\boldsymbol{X}})$, in addition to the displacement degrees of freedom, $\underline{\boldsymbol{U}}(\underline{\boldsymbol{X}})$. It is assumed that the development of microdeformation gradient

$$\underline{\underline{\boldsymbol{K}}}(\underline{\boldsymbol{X}}) := \underline{\underline{\boldsymbol{\chi}}}(\underline{\boldsymbol{X}}) \otimes \boldsymbol{\nabla}_X \tag{2}$$

is associated with internal work and energy storage. There is also an energetic price to pay for the microdeformation to depart from the macrodeformation, characterized by the relative deformation measure

$$\underline{\underline{\boldsymbol{e}}}(\underline{\boldsymbol{X}}) := \underline{\boldsymbol{U}}(\underline{\boldsymbol{X}}) \otimes \boldsymbol{\nabla}_X - \underline{\underline{\boldsymbol{\chi}}}(\underline{\boldsymbol{X}}) \tag{3}$$

The substitution of a heterogeneous Cauchy material by a homogeneous micromorphic medium requires the definition of the additional degrees of freedom as functions of the micro-fields. For a given local displacement field $\underline{\boldsymbol{u}}(\underline{\boldsymbol{x}})$ in the volume element V, it has been proposed in Forest (2002); Forest and Sab (1998); Forest and Trinh (2011); Jänicke

and Diebels (2009) and Jänicke et al. (2009) to determine the homogeneous deformation field that is the closest to the actual displacement field, in the sense of the following minimization problem:

$$\min_{\underline{\boldsymbol{U}}(\underline{\boldsymbol{X}}),\underset{\sim}{\boldsymbol{\chi}}(\underline{\boldsymbol{X}})} \int_V \left|\left|\underline{\boldsymbol{u}}(\underline{\boldsymbol{x}}) - \underline{\boldsymbol{U}}(\underline{\boldsymbol{X}}) - \underset{\sim}{\boldsymbol{\chi}}(\underline{\boldsymbol{X}}) \cdot (\underline{\boldsymbol{x}} - \underline{\boldsymbol{X}})\right|\right|^2 dV \tag{4}$$

for a given material point $\underline{\boldsymbol{X}}$. The minimization procedure is straightforward and delivers, taking $\underline{\boldsymbol{X}}$ as the center of $V(\underline{\boldsymbol{X}})$

$$\underline{\boldsymbol{U}}(\underline{\boldsymbol{X}}) = \langle \underline{\boldsymbol{u}}(\underline{\boldsymbol{x}}) \rangle_V, \quad \underset{\sim}{\boldsymbol{A}} = \langle (\underline{\boldsymbol{x}} - \underline{\boldsymbol{X}}) \otimes (\underline{\boldsymbol{x}} - \underline{\boldsymbol{X}}) \rangle_V \tag{5}$$

$$\underset{\sim}{\boldsymbol{\chi}}(\underline{\boldsymbol{X}}) = \langle [\underline{\boldsymbol{u}}(\underline{\boldsymbol{x}}) - \underline{\boldsymbol{U}}(\underline{\boldsymbol{X}})] \otimes (\underline{\boldsymbol{x}} - \underline{\boldsymbol{X}}) \rangle_V . \underset{\sim}{\boldsymbol{A}}^{-1} = \langle \underline{\boldsymbol{u}}(\underline{\boldsymbol{x}}) \otimes (\underline{\boldsymbol{x}} - \underline{\boldsymbol{X}}) \rangle_V . \underset{\sim}{\boldsymbol{A}}^{-1} \tag{6}$$

where the quadratic moment $\underset{\sim}{\boldsymbol{A}}$ is introduced and assumed to be macroscopically uniform in the sequel. The definition of the overall continuum then requires the evaluation of the macroscopic gradients of the degrees of freedom. The macroscopic gradient of the displacement field is still given by the average (12). The gradient of the microdeformation (2) is computed using the definition (6) as follows (Forest and Trinh, 2011):

$$\underset{\sim}{\boldsymbol{K}}^T(\underline{\boldsymbol{X}}) = \langle [\underline{\boldsymbol{u}}(\underline{\boldsymbol{x}}) \otimes \boldsymbol{\nabla}_x] \otimes (\underline{\boldsymbol{x}} - \underline{\boldsymbol{X}}) \rangle \cdot \underset{\sim}{\boldsymbol{A}}^{-1}, \quad K_{ijk} = \langle u_{i,k}(x_l - X_l) \rangle A^{-1}_{lj} \tag{7}$$

where transposition of the third rank tensor is applied to the last two indices. Accordingly, the microdeformation gradient can be interpreted as the first moment of the distribution of the local displacement gradient. The relative deformation must also be evaluated and takes the form of the difference

$$\underset{\sim}{\boldsymbol{e}}(\underline{\boldsymbol{X}}) = \langle \underline{\boldsymbol{u}}(\underline{\boldsymbol{x}}) \otimes \boldsymbol{\nabla}_x \rangle_V - \langle \underline{\boldsymbol{u}}(\underline{\boldsymbol{x}}) \otimes (\underline{\boldsymbol{x}} - \underline{\boldsymbol{X}}) \rangle_V \cdot \underset{\sim}{\boldsymbol{A}}^{-1} \tag{8}$$

When the displacement field $\underline{\boldsymbol{u}}$ is an affine transformation, including a rigid-body motion, both the relative deformation and the microdeformation gradient vanish, as it should be.

The overall micromorphic continuum is characterized by the form of the power density of internal forces, which involves three stress tensors, the dual quantities of the previous three kinds of strain measures

$$p^{(i)}(\underline{\boldsymbol{U}}, \underset{\sim}{\boldsymbol{\chi}}) := \underset{\sim}{\boldsymbol{\Sigma}} : \underline{\boldsymbol{U}} \otimes \boldsymbol{\nabla}_X + \underset{\sim}{\boldsymbol{S}} : \underset{\sim}{\boldsymbol{e}} + \underline{\underline{\boldsymbol{M}}} \vdots \underset{\sim}{\boldsymbol{\chi}} \otimes \boldsymbol{\nabla}_X = \langle \underset{\sim}{\boldsymbol{\sigma}} : \underset{\sim}{\boldsymbol{\varepsilon}} \rangle \tag{9}$$

The simple force stress tensor $\underset{\sim}{\boldsymbol{\Sigma}}$ is taken symmetric, whereas the relative stress tensor $\underset{\sim}{\boldsymbol{S}}$ is generally not symmetric. The double stress tensor $\underline{\underline{\boldsymbol{M}}}$ does not display in general any symmetry property with respect to its three indices.

2.2 Second Gradient Overall Continuum

The second gradient model relies on the introduction of the first and second gradients of the displacement field, $\underline{\boldsymbol{U}}(\underline{\boldsymbol{X}})$, in the continuum model. In particular, the work density of internal forces takes the following form:

$$p^{(i)}(\underline{\boldsymbol{U}}) := \underset{\sim}{\boldsymbol{\Sigma}} : \underline{\boldsymbol{U}} \otimes \boldsymbol{\nabla}_X + \underline{\underline{\boldsymbol{M}}} \vdots \underline{\boldsymbol{U}} \otimes \boldsymbol{\nabla}_X \otimes \boldsymbol{\nabla}_X \tag{10}$$

where $\underset{\sim}{\boldsymbol{\Sigma}}$ is the symmetric simple stress tensor and $\underline{\underline{\boldsymbol{M}}}$ the hyperstress or double stress tensor, which is symmetric with respect to its two last indices. Note that there is a strict equivalence between the strain gradient and the second gradient of displacement models (Mindlin and Eshel, 1968). The stress tensors fulfill the following balance of momentum equation:

$$\underset{\sim}{\boldsymbol{\tau}} \cdot \boldsymbol{\nabla}_X = 0, \quad \text{with} \quad \underset{\sim}{\boldsymbol{\tau}} = \underset{\sim}{\boldsymbol{\Sigma}} - \underline{\underline{\boldsymbol{M}}} \cdot \boldsymbol{\nabla}_X \tag{11}$$

in the absence of volume forces nor acceleration. Constitutive relationships relate the first and second gradient of displacement to both stress tensors.

The macroscopic displacements, strain, and strain gradients are the mean values of the local strain and strain gradient over a material volume element, V, made of a Cauchy heterogeneous material (Forest and Trinh, 2011)

$$\underline{\boldsymbol{U}}(\underline{\boldsymbol{X}}) = \langle \underline{\boldsymbol{u}}(\underline{\boldsymbol{x}}) \rangle_V, \quad \underline{\boldsymbol{U}} \otimes \boldsymbol{\nabla}_X = \langle \underline{\boldsymbol{u}} \otimes \boldsymbol{\nabla}_x \rangle_V \tag{12}$$

$$\underset{\sim}{\boldsymbol{K}} := \underline{\boldsymbol{U}} \otimes \boldsymbol{\nabla}_X \otimes \boldsymbol{\nabla}_X = \langle \underline{\boldsymbol{u}}\,(\underline{\boldsymbol{x}}\,) \otimes \boldsymbol{\nabla}_x \otimes \boldsymbol{\nabla}_x \rangle_V \tag{13}$$

The main difference between the strain measures $\underset{\sim}{\boldsymbol{K}}$ in the second gradient and micromorphic models is that $\underset{\sim}{\boldsymbol{K}}$ is symmetric with respect to the last two indices in the former case.

The identification of the micromorphic substitution medium properties proceeds through the identification of the macro-energy density and the averaged energy in V

$$\langle \underset{\sim}{\boldsymbol{\sigma}} : \underset{\sim}{\boldsymbol{\varepsilon}} \rangle_V = \underset{\sim}{\boldsymbol{\Sigma}}(\underline{\boldsymbol{X}}\,) : \underset{\sim}{\boldsymbol{E}}(\underline{\boldsymbol{X}}\,) + \underset{\sim}{\boldsymbol{M}}(\underline{\boldsymbol{X}}\,) \vdots \underset{\sim}{\boldsymbol{K}}(\underline{\boldsymbol{X}}\,) \tag{14}$$

where $\underset{\sim}{\boldsymbol{E}}$ is the symmetric part of the displacement gradient. The micromorphic model encompasses the strain gradient theory as a limit case if the internal constraint

$$\underset{\sim}{\boldsymbol{\chi}} \equiv \underline{\boldsymbol{U}} \otimes \boldsymbol{\nabla}_X \quad \Longleftrightarrow \quad \underset{\sim}{\boldsymbol{e}} \equiv 0 \tag{15}$$

is enforced (Forest, 2009).

2.3 Cosserat Overall Continuum

The Cosserat model is a special case of the micromorphic theory for which the microdeformation reduces to a pure microrotation, meaning that microstrains are considered to be inactive. It amounts to limiting the minimization (4) to skew-symmetric $\underset{\sim}{\boldsymbol{\chi}}$ or, equivalently, to axial vectors $\underline{\boldsymbol{\Phi}}$, as proposed in Forest and Sab (1998)

$$\min_{\underline{\boldsymbol{U}}\,(\underline{\boldsymbol{X}}\,),\underline{\boldsymbol{\Phi}}\,(\underline{\boldsymbol{X}}\,)} \int_V ||\underline{\boldsymbol{u}}\,(\underline{\boldsymbol{x}}\,) - \underline{\boldsymbol{U}}\,(\underline{\boldsymbol{X}}\,) - \underline{\boldsymbol{\Phi}}\,(\underline{\boldsymbol{X}}\,) \times (\underline{\boldsymbol{x}} - \underline{\boldsymbol{X}}\,)||^2 \, dV \tag{16}$$

where $\times$ denotes the vector product. The same definition (5) follows for the macroscopic displacement. The macroscopic Cosserat rotation vector is solution of

$$(\operatorname{trace} \underset{\sim}{\boldsymbol{A}})\underline{\boldsymbol{\Phi}} + \int_V \underline{\boldsymbol{\Phi}} \cdot (\underline{\boldsymbol{x}} - \underline{\boldsymbol{X}}\,)(\underline{\boldsymbol{x}} - \underline{\boldsymbol{X}}\,)\, dV = \int_V (\underline{\boldsymbol{x}} - \underline{\boldsymbol{X}}\,) \times (\underline{\boldsymbol{u}} - \underline{\boldsymbol{U}}\,)\, dV \tag{17}$$

where the geometric tensor $\underset{\sim}{\boldsymbol{A}}$ has already been defined. The Cosserat deformation and curvature tensors are then defined as

$$\underset{\sim}{\boldsymbol{e}} := \underline{\boldsymbol{U}} \otimes \boldsymbol{\nabla}_X + \underset{\sim}{\boldsymbol{\varepsilon}} \cdot \underline{\boldsymbol{\Phi}}, \quad \underset{\sim}{\boldsymbol{K}} := \underline{\boldsymbol{\Phi}} \otimes \boldsymbol{\nabla}_X \tag{18}$$

The identification of the Cosserat substitution medium properties proceeds through the identification of the macro-energy density and the averaged energy in V

$$\langle \underset{\sim}{\boldsymbol{\sigma}} : \underset{\sim}{\boldsymbol{\varepsilon}} \rangle_V = \underset{\sim}{\boldsymbol{\Sigma}} : \underset{\sim}{\boldsymbol{e}}^{sym} + \underset{\sim}{\boldsymbol{S}} : \underset{\sim}{\boldsymbol{e}}^{skew} + \underset{\sim}{\boldsymbol{M}} \vdots \underset{\sim}{\boldsymbol{K}} \tag{19}$$

where $\underset{\sim}{\boldsymbol{\Sigma}}$ is the symmetric stress tensor, $\underset{\sim}{\boldsymbol{S}}$ is the skew-symmetric stress tensor, that work with the symmetric and skew-symmetric parts of the relative deformation, respectively, and $\underset{\sim}{\boldsymbol{M}}$ the couple-stress tensor.

In the two-dimensional case for a square unit cell with edge length l and with $\underline{\boldsymbol{X}}$ at the center, we derive from (17) the following formula:

$$\underline{\boldsymbol{\Phi}} = \frac{6}{l^2} \langle (\underline{\boldsymbol{x}} - \underline{\boldsymbol{X}}\,) \times (\underline{\boldsymbol{u}} - \underline{\boldsymbol{U}}\,) \rangle_V \tag{20}$$

which was given in Forest and Sab (1998) and is used in the present work. If the deformation plane is $(\underline{\boldsymbol{e}}_1, \underline{\boldsymbol{e}}_2)$ then $\underline{\boldsymbol{\Phi}} = \Phi_3 \underline{\boldsymbol{e}}_3$. As a result, only two components of the curvature tensor do not vanish, namely K_{31}, K_{32}:

$$K_{31} = \frac{6}{l^2} \langle x_1 u_{2,1} - x_2 u_{1,1} \rangle_V, \quad K_{32} = \frac{6}{l^2} \langle x_1 u_{2,2} - x_2 u_{1,2} \rangle_V \tag{21}$$

3. POLYNOMIAL LOADING CONDITIONS OF THE UNIT CELL

Polynomial loading conditions have been extensively used recently to develop generalized homogenization schemes. Various orders are considered depending on the chosen overall generalized continuum theory. We recall here three cases that are evaluated in Section 5 and we discuss the essential question of the existence of a RVE for such boundary conditions.

3.1 Selection of Polynomial Coefficients

The local displacement inside a volume element V of heterogeneous material can be expanded in the polynomial form

$$\underline{\boldsymbol{u}}\,(\underline{\boldsymbol{x}}\,) = \underset{\sim}{\boldsymbol{E}} \cdot \underline{\boldsymbol{x}} + \frac{1}{2}\underset{\approx}{\boldsymbol{D}} : (\underline{\boldsymbol{x}} \otimes \underline{\boldsymbol{x}}\,) + \frac{1}{3}\underset{\approx}{\boldsymbol{D}} \vdots (\underline{\boldsymbol{x}} \otimes \underline{\boldsymbol{x}} \otimes \underline{\boldsymbol{x}}\,) + \frac{1}{4}\underset{\approx}{\boldsymbol{D}} :: (\underline{\boldsymbol{x}} \otimes \underline{\boldsymbol{x}} \otimes \underline{\boldsymbol{x}} \otimes \underline{\boldsymbol{x}}\,) + \underline{\boldsymbol{v}}\,(\underline{\boldsymbol{x}}\,), \quad \forall \underline{\boldsymbol{x}} \in V \tag{22}$$

The coefficients of the polynomials are constant and exhibit the following symmetry properties: the components D_{ijk}, D_{ijkl} and D_{ijklm} are symmetric with respect to their two, three and four last indices, respectively. A fluctuation field $\underline{\boldsymbol{v}}\,(\underline{\boldsymbol{x}}\,)$ must be added for such an expansion to exist in general. Such polynomials can be used to inhomogeneously deform the material element V and therefore explore the heterogeneous material's response to various inhomogeneous deformation modes. How this polynomial loading is prescribed to the volume elements depends on the choice of the fluctuation field $\underline{\boldsymbol{v}}$ at the boundary ∂V of the volume elements. Some possible choices are discussed in Section 3.2.

The order of the polynomials to be retained in the expansion is directly related to the order of the overall generalized continuum theory as follows:

1. The quadratic contribution D_{ijk} is required for the identification of an overall second gradient medium (Forest and Trinh, 2011; Geers et al., 2001; Gologanu et al., 1997). Some components of the quadratic term corresponding to bending modes are sufficient for the construction of an overall couple-stress medium in Ostoja-Starzewski et al. (1999) and Bouyge et al. (2001).

2. Some components of the quadratic term D_{ijk} and of the third-order polynomial D_{ijkl} are involved in the construction of an effective Cosserat medium (Forest and Sab, 1998). The selection of the relevant coefficients was made by keeping only the ones that contribute to the overall microrotation and curvature of the unit cell as defined by (20) and (21), respectively.

3. Some components of the fourth-order polynomial D_{ijkm} are needed for a 3D Cosserat continuum (Forest, 2002) and for an overall micromorphic medium (Jänicke et al., 2009). The selection of the relevant coefficients is discussed in these contributions.

3.2 Role of Fluctuation Field

Imposing a mean curvature or mean strain gradient to a volume element can be done in various ways related to the choice of the fluctuation $\underline{\boldsymbol{v}}$ in (22). The procedures presented in the literature are not completely satisfactory yet, as discussed in Forest and Trinh (2011). Three main possibilities have been exploited:

1. $\underline{\boldsymbol{v}}\,(\underline{\boldsymbol{x}}\,) = 0, \forall \underline{\boldsymbol{x}} \in \partial V$. The fluctuation is set to zero at the boundary of the volume elements. As a result, the displacement is polynomial at the boundary of V. This is a straightforward method that has been shown to deliver reasonable estimates of effective properties for generalized substitution medium. However, it suffers from two limitations. First it cannot be used to impose strictly a given mean strain gradient because strain cannot be prescribed at the boundary. Let us illustrate this point in a simple case where only the coefficient D_{111} is considered

$$u_1 = \frac{1}{2} D_{111} x_1^2, \quad u_2 = 0, \quad \forall \underline{\boldsymbol{x}} \in \partial V \tag{23}$$

We compute the average second gradient component

$$\langle u_{1,11} \rangle = \frac{1}{V} \int_V u_{1,11}\, dV = \frac{1}{V} \int_{\partial V} u_{1,1} n_1\, dS \tag{24}$$

This expression cannot be further exploited because the strain component $\varepsilon_{11} = u_{1,1}$ is not known on the whole boundary ∂V, even though u_1 is known. The strain cannot be prescribed at the boundary in a Cauchy continuum. In contrast, Eq. (7) can be used and delivers

$$\begin{aligned} K_{111} &= \frac{12}{l^2 V}\int_V u_{1,1}x_1\,dV = \frac{12}{l^2 V}\int_V (u_1x_1)_{,1}\,dV - \frac{12}{l^2}\langle u_1\rangle = \frac{12}{l^2 V}\int_{\partial V} u_1x_1n_1\,dS - \frac{12}{l^2}\langle u_1\rangle \\ &= \frac{12}{l^2 V}\int_{\partial V}\frac{1}{2}D_{111}x_1^3n_1dS - \frac{12}{l^2}\langle u_1\rangle = \frac{12}{l^2 V}\frac{3}{2}D_{111}\int_V x_1^2\,dV - \frac{12}{l^2}\langle u_1\rangle = \frac{3}{2}D_{111} - \frac{12}{l^2}\langle u_1\rangle \end{aligned} \tag{25}$$

This expression shows that K_{111} is indeed related to the coefficient D_{111} but the second contribution is a priori unknown and can be obtained from a post-processing of the solution of the boundary value problem on the volume V. Second, as in classical homogenization (see section 4.2), prescribing Dirichlet conditions at the boundary of the volume element generally delivers too stiff effective moduli.

2. $\underline{\boldsymbol{v}}\,(\underline{\boldsymbol{x}}\,)$ is periodic at homologous points of a periodic unit cell. The periodicity constraint was imposed in Forest and Sab (1998) and Kouznetsova et al. (2004b). The periodicity constraint also requires the anti-periodicity of the stress vector at boundaries. The latter conditions enable simple definitions for the overall stress tensors based on Hill–Mandel conditions. However there is in general no reason for assuming such a periodicity requirement in the presence of overall strain gradient loading, as pointed out by Bacigalupo and Gambarotta (2010); Kaczmarczyk et al. (2008) and Yuan et al. (2008).

3. No constraint on $\underline{\boldsymbol{v}}$, as obtained at the boundary of a unit cell if the Dirichlet polynomial conditions are prescribed at the boundary of a periodic heterogeneous material far away from the considered unit cell, as proposed in Forest and Trinh (2011). This procedure is related to the concept of RVE for polynomial conditions discussed in Section 3.3. The convergence study with respect to the number of considered unit cells also confirmed in a special numerical case that the fluctuation $\underline{\boldsymbol{v}}$ is not periodic.

These various assumptions will be used in Section 4 to identify overall generalized elasticity moduli.

3.3 Existence of a RVE for Polynomial Boundary Conditions

The question of the existence of a representative volume element is essential for establishing a solid foundation for homogenization procedures. Let us consider a periodic microstructure with a unit cell V_0. In a three-dimensional space, a material volume element V can be built by tessellation of N^3 translated volumes V_0. The authors in Kouznetsova et al. (2004a) investigated the overall second gradient elastic moduli based on quadratic Dirichlet conditions for increasing values of N. They found that these moduli, as derived from the mean energy density computed in V for each loading, increase with N and do not converge towards unique effective properties. In Pham (2010), the author claims that this is a fundamental weakness of the method and proposes an alternative way of defining the effective moduli that do not depend on N. This is a significant step toward establishing solid foundations for the homogenization model. A different perspective is proposed in Forest and Trinh (2011). Instead of computing the overall energy density on V when increasing N, it is proposed to compute it on one single central unit cell. This energy level was found to converge for the loading conditions and the special unit cell geometry considered in Forest and Trinh (2011). As a result, the fluctuation field $\underline{\boldsymbol{v}}$ at the boundary of V_0 was determined exactly. It did not display the usual periodicity properties. This technique is used in Section 4 to check whether such a convergence exists for the considered test material and whether effective moduli can be determined in that way.

In particular, the analysis of the fluctuation field after convergence of the RVE size in Forest and Trinh (2011) shows that the fluctuation generally contributes to the mean second gradient of the displacement field so that the latter differs from the coefficients of the quadratic term in the polynomial expansion. In contrast, the boundary conditions proposed in Kaczmarczyk et al. (2008) assume that the mean average second gradient of the fluctuation vanishes. The fluctuation field obtained from convergence analysis in Forest and Trinh (2011) should be compared to the fluctuation field proposed in Bacigalupo and Gambarotta (2010) and Yuan et al. (2008).

4. IDENTIFICATION OF GENERALIZED EFFECTIVE ELASTIC MODULI

4.1 Definition of the Chosen Composite Material

The chosen periodic composite material for the evaluation of the extended homogenization methods is made of a hard isotropic linear elastic phase (h) and a soft isotropic linear elastic phase (s)

$$E^h = 100\,000\,\mathrm{MPa}, \quad \nu^h = 0.3, \quad E^s = 500\,\mathrm{MPa}, \quad \nu^s = 0.3$$

The two phases display a contrast of 200 in their Young's modulus. The retained two-dimensional geometry of the unit cell V_0 of the periodic composite is shown in Fig. 1(a). It exhibits orthotropic symmetry. The volume fraction of the hard phase is $f^h = 0.424$. The whole microstructure is obtained by plane tessellation in the defined directions 1 and 2. A second possible unit cell leading to the same material by tessellation is given in Fig. 1(b). It will be used to test the influence of the choice of the unit cell on the predicted generalized effective properties.

4.2 Identification of Classical Elastic Moduli

Classical periodic homogenization is used to compute the orthotropic elastic properties of the effective Cauchy material. A constant mean deformation gradient E_{ij} is applied to the unit cell in which the displacement field is of the form :

$$\underline{\boldsymbol{u}}\,(\underline{\boldsymbol{x}}\,) = \underset{\sim}{\boldsymbol{E}} \cdot \underline{\boldsymbol{x}} + \underline{\boldsymbol{v}}\,(\underline{\boldsymbol{x}}\,) \tag{26}$$

where $\underline{\boldsymbol{v}}$ is the periodic displacement fluctuation taking identical values at homologous points of the boundary ∂V_0 of the unit cell. The effective moduli are determined from the mean elastic energy density induced by three successive independent loading conditions, as illustrated in Fig. 2. Finite element simulations are performed under plane strain conditions. The found moduli are provided in Table 1. They are defined in the following matrix form

$$\begin{bmatrix} \Sigma_{11} \\ \Sigma_{22} \\ \Sigma_{12} \end{bmatrix} = \begin{bmatrix} C_{11} & C_{12} & 0 \\ C_{12} & C_{22} & 0 \\ 0 & 0 & C_{44} \end{bmatrix} \begin{bmatrix} E_{11} \\ E_{22} \\ 2E_{12} \end{bmatrix} \tag{27}$$

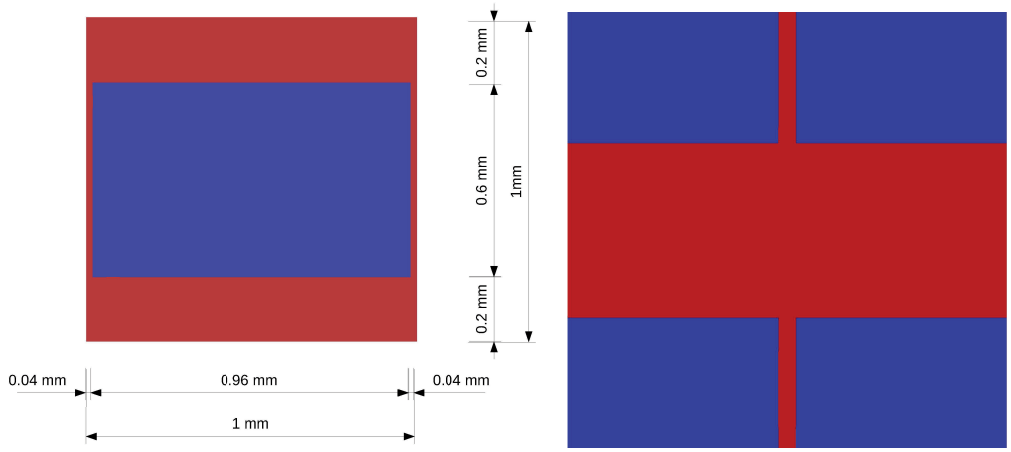

FIG. 1: Unit cell V_0 of the periodic composite material: **(a)** geometry of the unit cell and **(b)** second equivalent unit cell. The hard phase is red, and the soft phase is blue. The orthotropy axes 1 and 2 are respectively horizontal and vertical (See pdf version for color figures).

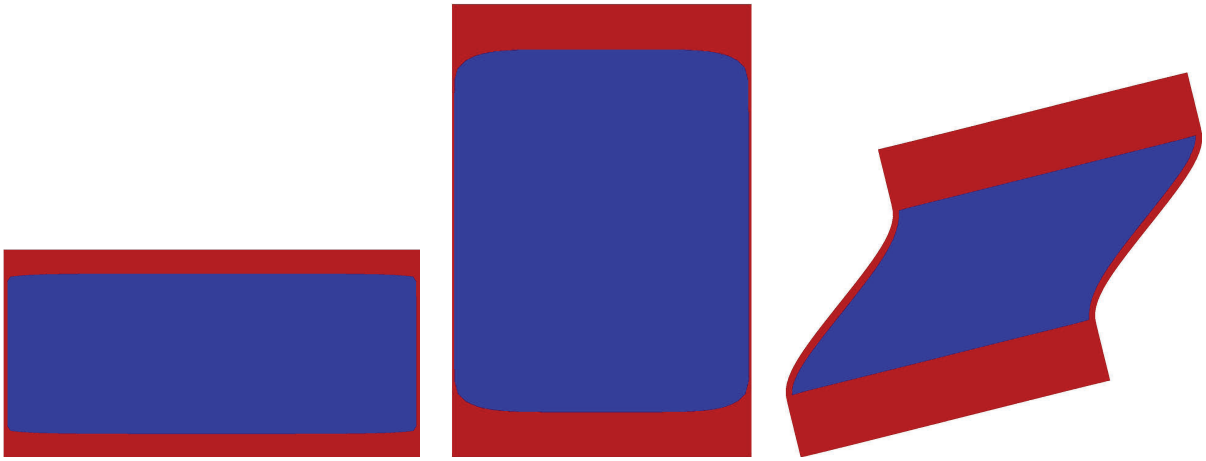

FIG. 2: Loading conditions applied to the unit cell for the determination of the effective properties of the homogeneous equivalent Cauchy material. The first, second, and third rows correspond to: $E_{11} = 1, E_{22} = 1, E_{12} = E_{21} = 0.25$, respectively. In each case, the remaining components of E_{ij} vanish.

TABLE 1: Elastic properties of the effective Cauchy material

	C_{11} (MPa)	C_{12} (MPa)	C_{22} (MPa)	C_{44} (MPa)
Periodic	44748	1579	7163	372
KUBC	45707	3181	9920	6186

As a comparison, we have also computed the apparent effective moduli when homogeneous deformation boundary conditions are applied to the unit cell, i.e., when the fluctuation is taken to vanish : $\underline{\boldsymbol{v}} = 0, \forall \underline{\boldsymbol{x}} \in \partial V_0$. These boundary conditions are referred to as, kinematic uniform boundary conditions (KUBC). The corresponding apparent moduli, also given in Table 1, are significantly stiffer than effective moduli from periodic homogenization, as expected (Kanit et al., 2003).

4.3 Identification of Cosserat Effective Elastic Moduli

The effective moduli of the overall Cosserat continuum are obtained by prescribing successively a mean curvature $\underset{\sim}{\boldsymbol{K}}$ and a mean relative deformation $\underset{\sim}{e}$ through polynomial conditions of the form

$$u_1^* = D_{222}x_2^2 - 2D_{111}x_1x_2 + D_3(x_2^3 - 3x_1^2x_2) + v_1(x_1, x_2) \tag{28}$$

$$u_2^* = D_{111}x_2^2 - 2D_{111}x_1x_2 - D_3(x_1^3 - 3x_1x_2^2) + v_2(x_1, x_2) \tag{29}$$

which represent a special case of (22) as proposed in Forest and Sab (1998). The mean curvature components K_{31} and K_{32} are directly related to the prescribed coefficients D_{111} and D_{222} by means of Eq. (21). The relative rotation $e_{12} - e_{21}$ is dictated by the value D_3 through Eq. (5), (18), and (20). The symmetric part $e_{12} + e_{21}$ corresponds to the classical engineering shear strain component $2E_{12}$ in Eq. (27).

The deformed states of the unit cell are shown in Fig. 3 where curvatures K_{31} and K_{32} are prescribed for three choices of the fluctuation fields, periodic, vanishing at the boundary or converged. This third type of fluctuation will be detailed in Section 4.4. The impact of the fluctuation is visible mainly for the curvature K_{32} due to the strong anisotropy of the chosen composite. The two deformed states corresponding to a prescribed relative rotation with periodic or vanishing fluctuations are shown in Fig. 4 (a) and 4(b).

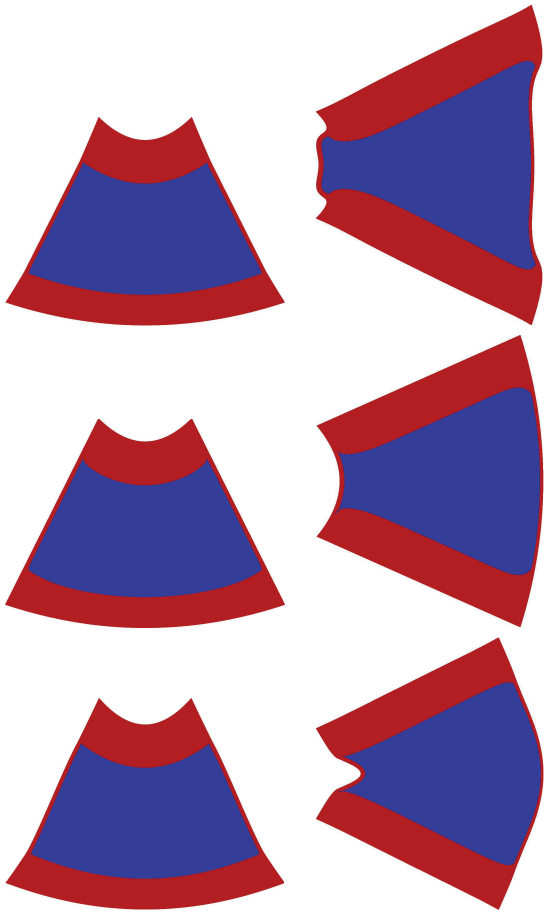

FIG. 3: Loading conditions applied to the unit cell for the determination of the effective bending properties of the homogeneous equivalent Cosserat medium. The three lines correspond respectively to periodic, vanishing, and converged fluctuation fields. The first and second columns are associated with prescribed curvature K_{31} and K_{32}, respectively.

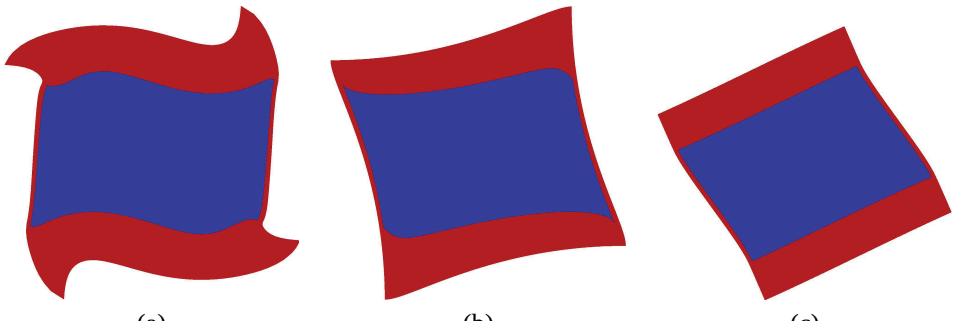

(a) (b) (c)

FIG. 4: Deformed state of the unit cell when a relative deformation is applied to the unit cell: **(a)** periodic boundary conditions, **(b)** no fluctuation, and **(c)** converged state.

The energy associated with each non-homogeneous deformation mode is used to identify the overall elastic moduli based on generalized Hill–Mandel condition (19). The skew-symmetric Cosserat stress component and the couple-stress component are linked to the relative deformation and curvature through the linear relationship

$$\begin{bmatrix} \Sigma_{12} \\ \Sigma_{21} \\ M_{31} \\ M_{32} \end{bmatrix} = \begin{bmatrix} Y_{1212} & Y_{1221} & 0 & 0 \\ Y_{1221} & Y_{2121} & 0 & 0 \\ 0 & 0 & C_{3131} & 0 \\ 0 & 0 & 0 & C_{3232} \end{bmatrix} \begin{bmatrix} e_{12} \\ e_{21} \\ K_{31} \\ K_{32} \end{bmatrix} \tag{30}$$

Orthotropic symmetry has been taken into account to write this matrix form. The corresponding moduli are determined from the energy contained in the presented deformed states and from the evaluation of Cosserat overall strain measures, all computed by means of a suited post-processing of the FE computations. The values of the found moduli are given in Table 2. The moduli C_{3131} and C_{3232} are obtained by applying D_{111} = 1 mm^{-1} and D_{222} = 1 mm^{-1} in (29), respectively. The corresponding curvatures are computed from the post-processing formula (21). They are found to differ depending on the fluctuation type. The found bending moduli are close. In contrast, the moduli controlling the skew-symmetric part of the overall stress significantly differ when the fluctuation is assumed to be periodic or taken to be zero.

The bending moduli C_{3131} and C_{3232} are also valid for an overall couple-stress medium for which the microrotation $\underline{\mathbf{\Phi}}$ is constrained to coincide with material rotation (Bouyge et al., 2001). Then, the combination of moduli intervening in the expression of the skew–symmetric part of the overall stress becomes a Lagrange multiplier.

The overall Cosserat and couple–stress properties can also be determined in the case of the alternative unit cell of Fig. 1(b), following the same procedure. The values put in Table 3 show a significant dependence of the generalized moduli, the cross morphology leading to significantly softer moduli.

4.4 RVE Size for Cosserat and Strain Gradient Overall Properties

The influence of the fluctuation type introduced in the boundary conditions in the computations of the previous section clearly shows that there is undoubtedly a boundary layer effect due to the polynomial boundary conditions. To get rid of the boundary layer effect, it is proposed to consider volume elements containing an increasing number of unit cells, typically a collection of N×N unit cells, with N = 1,3,5... up to N = 27 in the following simulations. We look for the size N for which the energy distribution in the bulk of the sample, defined as a zone of fixed size M×M, does not vary

TABLE 2: Elastic properties of the effective Cosserat material obtained for the unit cell of Fig. 1(a)

	Y_{1212} (MPa)	Y_{1221} (MPa)	Y_{2121} (MPa)	C_{3131} (K_{31}) [MPa mm^2 (mm^{-1})]	C_{3232} K_{32}) [MPa mm^2 (mm^{-1})]
Periodic	241250	–128383	69188	6788 (1.03)	2091 (0.9)
No fluctuation	976970	–616255	402759	5401 (1.17)	1502 (1.15)
Converged field	–	–	–	6004 (1.07)	878 (1.33)

TABLE 3: Elastic properties of the effective Cosserat material obtained for the unit cell of Fig. 1(b)

	Y_{1212} (MPa)	Y_{1221} (MPa)	Y_{2121} (MPa)	C_{3131} (K_{31}) [MPa mm^2 (mm^{-1})]	C_{3232} (K_{32}) [MPa mm^2 (mm^{-1})]
Periodic	2383	–3270	6966	630.4 (1.01)	930.7 (0.994)
No fluctuation	3695941	–5472478	8109835	651.1 (1.01)	955.6 (1.08)
Converged field	–	–	–	713 (1.07)	330 (0.58)

any more when the polynomial boundary conditions are applied at the remote boundary with the same given values of the polynomial coefficients. The obtained size will be called the RVE size for the considered polynomial conditions. In particular, the attention is focused on the energy density distribution inside the central unit cell (M = 1).

In the case of affine boundary conditions used for classical homogenization, such a procedure is known to lead to a stabilized periodic stress-strain field in the bulk of the volume element. In particular, the fluctuation at the boundary of a unit cell, defined as the difference between the displacement field and the affine contribution, is then found to be periodic.

For more general polynomial Dirichlet conditions prescribed at the outer, we can investigate the convergence of the mechanical fields for an increasing window size. We also define, in a similar way, the fluctuation $\underline{\boldsymbol{v}}$ and examine its properties at the boundary of the central unit cell. This program has been performed in Forest and Trinh (2011) for a cubic grid-like composite material for quadratic polynomials. We apply it to the orthotropic microstructure of Fig. 1 considered in this work. We use it also to determine the corresponding overall Cosserat and second gradient properties and compare them to the estimations based on an a priori choice of the fluctuation.

The Cosserat polynomial conditions (29), with $\underline{\boldsymbol{v}} = 0$, are prescribed at the outer boundary of a 15×15 cell volume element in Fig. 5. Clear bending can be seen in Figs. 5(a) and 5(b), whereas only a boundary layer seems to be affected by the third-order polynomial in Fig. 5(c) leaving the central cells rather undeformed. These computations have been performed from 1×1 up to 27×27 to check if a converged deformed state of the central cell is reached. These converged states are shown in the bottom of Fig. 3 for bending and Fig. 4(a). The converged bending modes are clearly identified, whereas the deformation of the central unit cell is close to a rigid-body rotation, when the third-order polynomial is applied.

The same strategy has been carried out in the case of the six 2D deformation modes corresponding to a full quadratic polynomial in Eq. (22): $D_{111}, D_{222}, D_{122}, D_{211}, D_{212}$, and D_{112}. The associated deformed 15×15–cell volume elements are shown in Fig. 6. The converged shapes of the central unit cell extracted from the previous volume elements are given in Fig. 7, for the same magnification. The modes D_{111}, D_{222}, and D_{122} induce only limited deformation in the central unit cell whereas D_{211}, D_{212}, and D_{112} involve significant straining. The elastic energy density levels $\langle \underset{\sim}{\boldsymbol{\sigma}} : \underset{\sim}{\boldsymbol{\varepsilon}} \rangle_{V_0}$ over the central unit cell V_0 associated with these six modes are given in Table 4 depending on the size N of the volume element. Convergence to finite energy values is obtained for the modes D_{211}, D_{212}, and D_{112} whereas the material turns out to be insensitive to the modes D_{111}, D_{222}, and D_{122}.

The displayed convergence for the considered collection of cells ensures that a representative size has been reached. However, quite a large number of cells is necessary to detect the energy-free modes. Detailed analysis confirms that the fluctuation corresponding to the central unit cell response is not periodic, as pointed out in Forest and Trinh (2011).

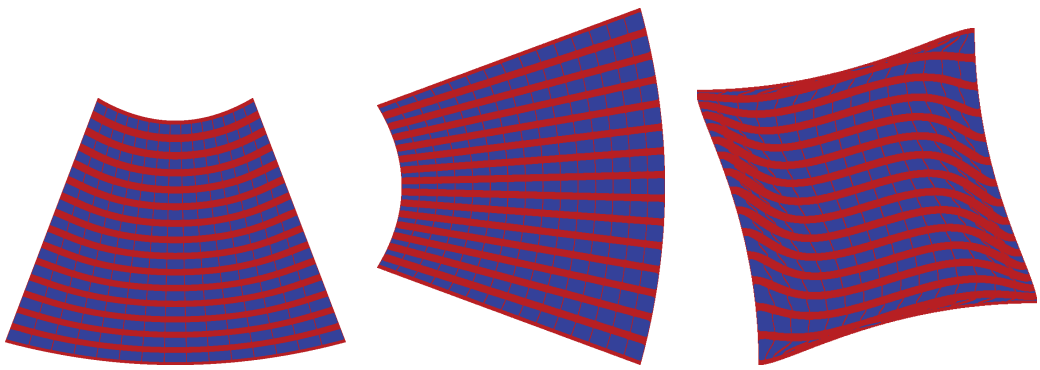

(a) (b) (c)

FIG. 5: Deformed states of a composite volume element containing 15×15 cells subjected to the polynomial conditions (29) with **(a)** $D_{111} = 1$ mm^{-1}, **(b)** $D_{222} = 1$ mm^{-1} and **(c)** $D_3 = 1$, the remaining coefficients being set to zero.

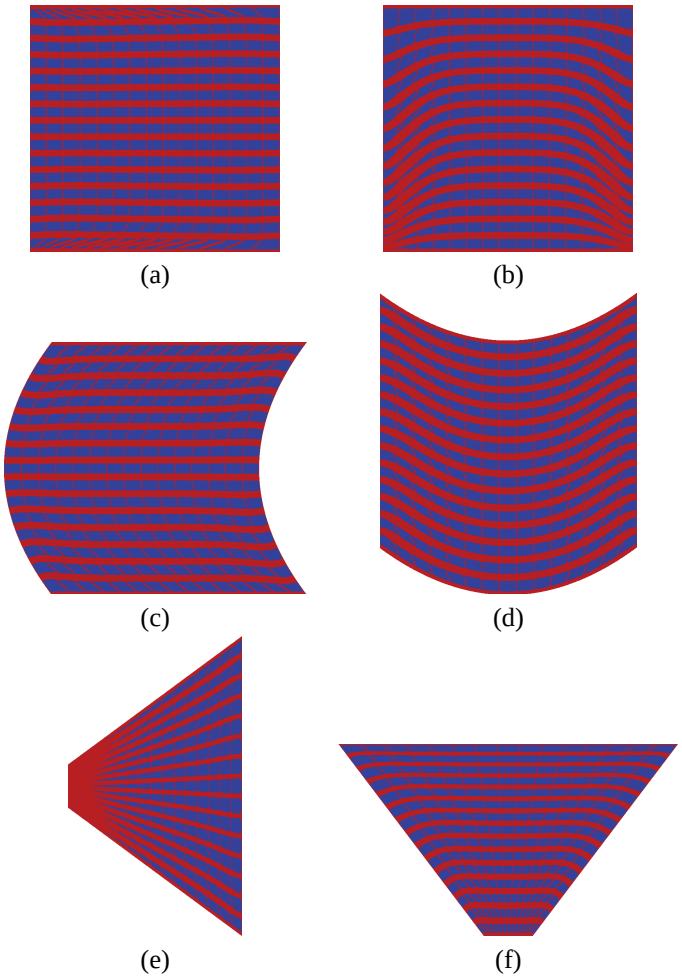

FIG. 6: Deformation of a 15×15–cell volume elements corresponding to the following Dirichlet conditions at the outer boundary: **(a)** $D_{111} : \underline{\boldsymbol{u}} = 1/2x_1^2\underline{\boldsymbol{e}}_1$, **(b)** $D_{222} : \underline{\boldsymbol{u}} = 1/2x_2^2\underline{\boldsymbol{e}}_2$, **(c)** $D_{122} : \underline{\boldsymbol{u}} = 1/2x_2^2\underline{\boldsymbol{e}}_1$, **(d)** $D_{211} : \underline{\boldsymbol{u}} = 1/2x_1^2\underline{\boldsymbol{e}}_2$, **(e)** $D_{212} : \underline{\boldsymbol{u}} = x_1x_2\underline{\boldsymbol{e}}_2$, and **(f)** $D_{112} : \underline{\boldsymbol{u}} = x_1x_2\underline{\boldsymbol{e}}_1$.

TABLE 4: Average elastic energy density in the central unit of N×N–cell volume elements submitted to quadratic Dirichlet boundary conditions. The components D_{ijk} are given in mm^{-1} and the elastic energy values are in Mpa

N×N-cell	$\boldsymbol{D_{111}=1}$	$\boldsymbol{D_{122}=1}$	$\boldsymbol{D_{212}=1}$	$\boldsymbol{D_{112}=1}$	$\boldsymbol{D_{211}=1}$	$\boldsymbol{D_{222}=1}$
3x3	3	19	1033	527	368	324
7x7	2	0.12	789	6176	660	227
9x9	1.3	0.3	761	6079	565	89
11x11	0.9	0.4	759	5930	474	27
15x15	0.5	0.33	770	5714	371	1.8
21x21	0.4	0.32	776	5587	325	0.2
27x27	0.33	0.32	777	5548	315	0.2

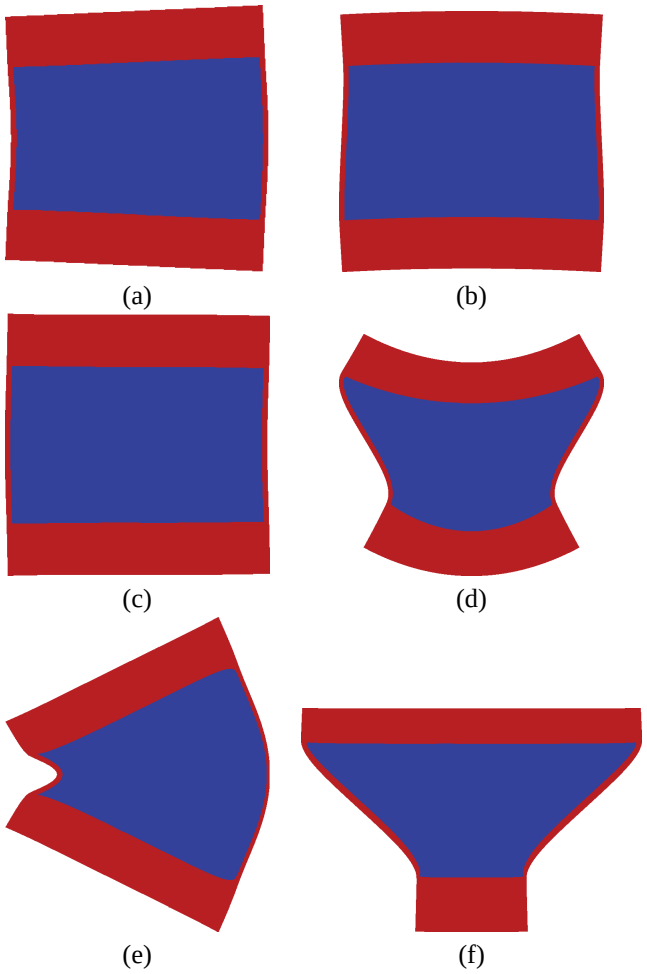

FIG. 7: Shape of the central cell of a 15×15 volume element subjected to the following Dirichlet boundary conditions: **(a)** D_{111} : $\underline{\boldsymbol{u}} = 1/2x_1^2\underline{\boldsymbol{e}}_1$, **(b)** D_{222} : $\underline{\boldsymbol{u}} = 1/2x_2^2\underline{\boldsymbol{e}}_2$, **(c)** D_{122} : $\underline{\boldsymbol{u}} = 1/2x_2^2\underline{\boldsymbol{e}}_1$, **(d)** D_{211} : $\underline{\boldsymbol{u}} = 1/2x_1^2\underline{\boldsymbol{e}}_2$, **(e)** D_{212} : $\underline{\boldsymbol{u}} = x_1x_2\underline{\boldsymbol{e}}_2$, and **(f)** D_{112} : $\underline{\boldsymbol{u}} = x_1x_2\underline{\boldsymbol{e}}_1$.

4.5 Identification of Second Gradient Effective Elastic Moduli

The quadratic polynomial loading conditions D_{ijk} can be used to identify the elastic properties of an overall second gradient medium. The simple force stress tensor $\underset{\sim}{\boldsymbol{\Sigma}}$ is still related to the strain tensor $\underset{\sim}{\boldsymbol{E}}$ by the moduli (27). In a medium exhibiting point symmetry, the double stress tensor $M_{ijk} = M_{ikj}$ is linearly related to the second gradient of displacement $K_{ijk} = K_{ikj}$ by the matrix of double elasticity moduli. The structure of anisotropic six rank tensors of strain gradient elasticity was analyzed by Auffray et al. (2009, 2010). In the most general situation, the associated matricial representation is written as follows:

$$\begin{bmatrix} M_{111} \\ M_{122} \\ \sqrt{2}M_{212} \\ M_{222} \\ M_{211} \\ \sqrt{2}M_{121} \end{bmatrix} = \begin{bmatrix} A_{111111} & A_{111122} & \sqrt{2}A_{111212} & A_{111222} & A_{111211} & \sqrt{2}A_{111121} \\ A_{122111} & A_{122122} & \sqrt{2}A_{122212} & A_{122222} & A_{122211} & \sqrt{2}A_{122121} \\ \sqrt{2}A_{212111} & \sqrt{2}A_{212122} & 2A_{212122} & \sqrt{2}A_{212222} & \sqrt{2}A_{212211} & 2A_{212121} \\ A_{222111} & A_{222122} & \sqrt{2}A_{222212} & A_{222222} & A_{222211} & \sqrt{2}A_{222121} \\ A_{211111} & A_{211122} & \sqrt{2}A_{211212} & A_{211222} & A_{211211} & \sqrt{2}A_{211121} \\ \sqrt{2}A_{121111} & \sqrt{2}A_{121122} & 2A_{121212} & \sqrt{2}A_{121222} & \sqrt{2}A_{121211} & 2A_{121121} \end{bmatrix} \begin{bmatrix} K_{111} \\ K_{122} \\ \sqrt{2}K_{212} \\ K_{222} \\ K_{211} \\ \sqrt{2}K_{121} \end{bmatrix} \tag{31}$$

This notation, using square root of 2 before K_{212} and M_{212}, defines a true second-order tensorial representation of the sixth-order tensor of double elasticity. Ranking the components of the second gradient of displacement as proposed in the former matricial representation, leads, in the orthotropic case, to the uncoupled system

$$\begin{bmatrix} M_1 \\ M_2 \\ M_3 \\ M_4 \\ M_5 \\ M_6 \end{bmatrix} = \begin{bmatrix} A_{11} & A_{12} & A_{13} & 0 & 0 & 0 \\ A_{12} & A_{22} & A_{23} & 0 & 0 & 0 \\ A_{13} & A_{23} & A_{33} & 0 & 0 & 0 \\ 0 & 0 & 0 & A_{44} & A_{45} & A_{46} \\ 0 & 0 & 0 & A_{45} & A_{55} & A_{56} \\ 0 & 0 & 0 & A_{46} & A_{56} & A_{66} \end{bmatrix} \begin{bmatrix} K_1 \\ K_2 \\ K_3 \\ K_4 \\ K_5 \\ K_6 \end{bmatrix} \tag{32}$$

with the simplified notations

$$[K_1 \quad K_2 \quad K_3 \quad K_4 \quad K_5 \quad K_6] = \begin{bmatrix} K_{111} & K_{122} & \sqrt{2}K_{212} & K_{222} & K_{211} & \sqrt{2}K_{121} \end{bmatrix} \tag{33}$$

$$[M_1 \quad M_2 \quad M_3 \quad M_4 \quad M_5 \quad M_6] = \begin{bmatrix} M_{111} & M_{122} & \sqrt{2}M_{212} & M_{222} & M_{211} & \sqrt{2}M_{121} \end{bmatrix} \tag{34}$$

and

$$[A_{11} \quad A_{12} \quad A_{13} \quad A_{22} \quad A_{23} \quad A_{33}] = \begin{bmatrix} A_{111111} & A_{111122} & \sqrt{2}A_{111212} & A_{122122} & \sqrt{2}A_{122212} & 2A_{212212} \end{bmatrix} \tag{35}$$

$$[A_{44} \quad A_{45} \quad A_{46} \quad A_{55} \quad A_{56} \quad A_{66}] = \begin{bmatrix} A_{222222} & A_{222211} & \sqrt{2}A_{222121} & A_{211211} & \sqrt{2}K_{211121} & 2K_{121121} \end{bmatrix} \tag{36}$$

This makes 12 independent double elasticity moduli to be identified from the analysis of the response of the unit cell to nonhomogeneous loading conditions. Twelve loading conditions are needed to identify them corresponding to 12 sets of the values of the coefficients D_{ijk}. The six selected loading conditions are labeled (a, b, c, d, e, f) for the identification of the first block of six constants in the matrix (32), taking advantage of the orthotropic symmetry of the material. Six additional ones are needed for the second block. For each loading, the post-processing procedure yields the mean energy density $2\epsilon = \langle \underset{\sim}{\boldsymbol{\sigma}} : \underset{\sim}{\boldsymbol{\xi}} \rangle_{V_0}$ in the unit cell and the overall curvature K_1, K_2, and K_3. The mean energy density is related to the overall energy density in the form

$$2\epsilon = \begin{bmatrix} K_1 & K_2 & K_3 & K_4 & K_5 & K_6 \end{bmatrix} \begin{bmatrix} A_{11} & A_{12} & A_{13} & 0 & 0 & 0 \\ A_{12} & A_{22} & A_{23} & 0 & 0 & 0 \\ A_{13} & A_{23} & A_{33} & 0 & 0 & 0 \\ 0 & 0 & 0 & A_{44} & A_{45} & A_{46} \\ 0 & 0 & 0 & A_{45} & A_{55} & A_{56} \\ 0 & 0 & 0 & A_{46} & A_{56} & A_{66} \end{bmatrix} \begin{bmatrix} K_1 \\ K_2 \\ K_3 \\ K_4 \\ K_5 \\ K_6 \end{bmatrix} \tag{37}$$

The six energy levels yield the following system of equations to solve for the higher order elastic moduli:

$$\begin{bmatrix} 2\epsilon_a \\ 2\epsilon_b \\ 2\epsilon_c \\ 2\epsilon_d \\ 2\epsilon_e \\ 2\epsilon_f \end{bmatrix} = \begin{bmatrix} K_{1a}^2 & K_{2a}^2 & K_{3a}^2 & 2\,K_{1a}\,K_{2a} & 2\,K_{2a}\,K_{3a} & 2\,K_{1a}\,K_{3a} \\ K_{1b}^2 & K_{2b}^2 & K_{3b}^2 & 2\,K_{1b}\,K_{2b} & 2\,K_{2b}\,K_{3b} & 2\,K_{1b}\,K_{3b} \\ K_{1c}^2 & K_{2c}^2 & K_{3c}^2 & 2\,K_{1c}\,K_{2c} & 2\,K_{2c}\,K_{3c} & 2\,K_{1c}\,K_{3c} \\ K_{1d}^2 & K_{2d}^2 & K_{3d}^2 & 2\,K_{1d}\,K_{2d} & 2\,K_{2d}\,K_{3d} & 2\,K_{1d}\,K_{3d} \\ K_{1e}^2 & K_{2e}^2 & K_{3e}^2 & 2\,K_{1e}\,K_{2e} & 2\,K_{2e}\,K_{3e} & 2\,K_{1e}\,K_{3e} \\ K_{1f}^2 & K_{2f}^2 & K_{3f}^2 & 2\,K_{1f}\,K_{2f} & 2\,K_{2f}\,K_{3f} & 2\,K_{1f}\,K_{3f} \end{bmatrix} \begin{bmatrix} A_{11} \\ A_{22} \\ A_{33} \\ A_{12} \\ A_{23} \\ A_{13} \end{bmatrix} \tag{38}$$

A similar system exists when K_4, K_5, and K_6 are activated.

The found higher order moduli are listed in Table 5 for a vanishing fluctuation $\underline{\boldsymbol{v}}$ in Eq. (22) at the boundary of the unit cell V_0. We have not determined the effective moduli corresponding to the converged states of the unit cell embedded in a N×N–cell volume element in the sense of Section 4.4, because zero-energy modes were detected as discussed above, so that the previous system of equations is undetermined. A specific procedure is necessary to determine the vanishing terms of the overall matrix, which has been addressed in Bacigalupo and Gambarotta (2010).

The higher order moduli obtained from the previous procedure are found to be very high in comparison to the Cosserat bending moduli.

TABLE 5: Higher order elastic properties of the overall second-gradient material for the unit cell of Fig. 1(a). The fluctuation is taken to vanish at the cell boundary

	$\boldsymbol{A_{11}}$ **(MPa mm^2)**	$\boldsymbol{A_{22}}$ **(MPa mm^2)**	$\boldsymbol{A_{33}}$ **(MPa mm^2)**	$\boldsymbol{A_{12}}$ **(MPa mm^2)**	$\boldsymbol{A_{23}}$ **(MPa mm^2)**	$\boldsymbol{A_{13}}$ **(MPa mm^2)**
No fluctuation	134601	37436	124 548	68706	67368	127 213
	A_{44}	A_{55}	A_{66}	A_{45}	A_{46}	A_{56}
No fluctuation	69445	2801	32 175	40762	11 094	7 548

4.6 Identification of Micromorphic Effective Elastic Moduli

In order to obtain the effective moduli of the overall micromorphic medium a cubic polynomial of the form

$$\begin{aligned} u_i^* = &\left(U_{i,1} - \frac{5}{2}\,e_{i1}\right) x_1 + \left(U_{i,2} - \frac{5}{2}\,e_{i2}\right) x_2 + \frac{10}{l^2}\,e_{i1}\,x_1^3 + \frac{10}{l^2}\,x_2^3 \\ &+\frac{1}{2}D_{i11}\,x_1^2 + \frac{1}{2}(D_{i12}+D_{i21})\,x_1x_2 + \frac{1}{2}D_{i22}\,x_2^2 - \frac{l^2}{24}(D_{i11}+D_{i22}) \end{aligned} \tag{39}$$

is introduced with the length of the unit cell l = 1 mm. This is in analogy to Jänicke (2010), where this type of polynomial has been applied to cellular periodic unit cells. We distinguish on the one hand between the even polynomial links (i.e., constant and quadratic ones), driven by the coefficients D_{ijk} and the odd polynomial links, controlled by the displacement gradient and the relative deformation, on the other. The constant part of the polynomial represents a rigid-body translation of the volume element and ensures the volume centroid to stay at a fixed position during deformation due to D_{ijk}. The coefficients of the quadratic part are assumed to be symmetric with respect to the last two indices $D_{ijk} = D_{ikj}$. By assumption, the cubic polynomial link has been restricted to the components depending on x_i^3. Hence, no mixed cubic terms are taken into account. Identification of the polynomial coefficients by means of the averaging rules (2) and (3) leads to the result that the cubic polynomial link is stimulated by the relative deformation, where the linear part depends on both, the relative deformation as well as the overall displacement gradient. We now make the simplification that the local field $\underline{\boldsymbol{u}}$ inside the unit cell is entirely given by Eq. (39), thus neglecting the fluctuation in Eq. (22). In that case, we find

$$K_{ijk} = D_{ijk} \tag{40}$$

Following this approximation, the Hill–Mandel identification (9) provides the explicit definition of the higher order stresses:

$$M_{ijk} = \langle \sigma_{i(j} x_{k)} \rangle \tag{41}$$

where the parentheses in the indices denote symmetrization with respect to the corresponding indices. Note that the chosen polynomial (39) does not allow to distinguish K_{ijk} from K_{ikj} although this should be necessary for the identification of a full micromorphic continuum. This is however not attempted here for the sake of brevity.

Several representative deformed states of the unit cell depending on $U_{i,j}$ and e_{ij} are given in Fig. 8. Evaluation of the generalized Hill-Mandel condition (9) allows for identification of the overall elastic moduli. Taking into account orthotropic symmetry, the components of the symmetric force stress tensor $\underset{\sim}{\boldsymbol{\Sigma}}$ and the relative stress tensor $\underset{\sim}{\boldsymbol{S}}$ are calculated as follows:

$$\begin{bmatrix} \Sigma_{11} \\ \Sigma_{22} \\ S_{11} \\ S_{22} \end{bmatrix} = \begin{bmatrix} Y_{1111} & Y_{1122} & Z_{1111} & Z_{1122} \\ Y_{1122} & Y_{2222} & Z_{2211} & Z_{2222} \\ \eta_{1111} & \eta_{1122} & \zeta_{1111} & \zeta_{1122} \\ \eta_{2211} & \eta_{2222} & \zeta_{1122} & \zeta_{2222} \end{bmatrix} \begin{bmatrix} u_{1,1} \\ u_{2,2} \\ e_{11} \\ e_{22} \end{bmatrix}, \tag{42}$$

$$\begin{bmatrix} \Sigma_{12} \\ S_{12} \\ S_{21} \end{bmatrix} = \begin{bmatrix} Y_{1212} & Y_{1212} & Z_{1212} & Z_{1221} \\ \eta_{1212} & \eta_{1212} & \zeta_{1212} & \zeta_{1221} \\ \eta_{2112} & \eta_{2112} & \zeta_{1221} & \zeta_{2121} \end{bmatrix} \begin{bmatrix} u_{1,2} \\ u_{2,1} \\ e_{12} \\ e_{21} \end{bmatrix}. \tag{43}$$

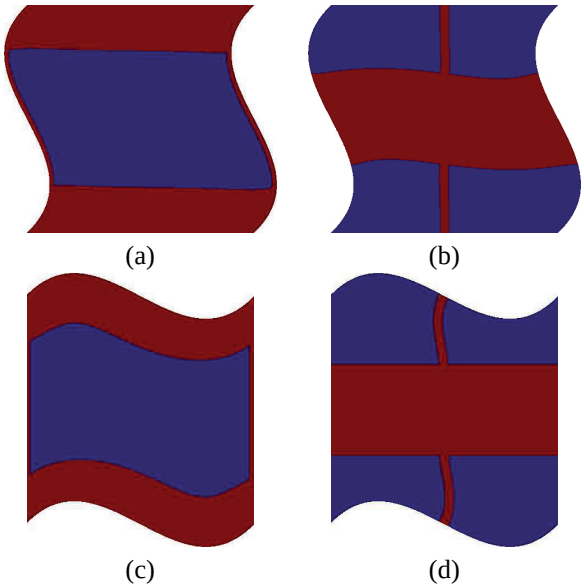

FIG. 8: Loading conditions applied to the different unit cell for the determination of the effective properties of the homogeneous equivalent micromorphic medium: **(a)** and **(c)** $\underline{\boldsymbol{u}} = (-5/2\, x_1 + 10/l^2\, x_1^3)\, e_{12}\, \underline{\boldsymbol{e}}_1$, **(b)** and **(d)** $\underline{\boldsymbol{u}} = (-5/2\, x_2 + 10/l^2\, x_2^3)\, e_{21}\, \underline{\boldsymbol{e}}_2$.

The matrix of higher order moduli for the calculation of double stresses is identical to relation (32) when the skew–symmetric part of K_{ijk} with respect to its two last indices is overlooked. The particular elastic moduli are given explicitely in Table 6 for both configurations of the unit-cell 1(a) and (b).

The found higher order moduli determined from this simplified scheme are found to be significantly smaller than those in Table 5. Their magnitude is comparable to the Cosserat bending moduli. As it has been observed for the Cosserat overall continuum, the cross morphology of Fig. 1(b) leads to elastic moduli significantly softer compared to the first morphology Fig. 1(a).

5. VALIDATION OF EXTENDED HOMOGENIZATION METHOD

The performance of the various generalized overall properties determined in Section 4 is evaluated by considering a reference problem for a structure made of a small number of unit cells of the type of Fig. 1(a). The limitation of the Cauchy continuum is first illustrated, and improvements by means of Cosserat, second gradient, and micromorphic substitution media are presented.

5.1 Reference Structural Computation and Limitations of the Cauchy Approach

We consider the composite structure made of 10×5 cells of Fig. 9(a). The following boundary value problem is considered on this structure. The left side of the structure is clamped, meaning that $U_1 = U_2 = 0$. The horizontal lower and upper sides are free of forces. The vertical displacement component U_2 = 1 mm is prescribed on the right side, the component U_1 being left free. The corresponding deformed shape of structure is shown in Fig. 9(b). It displays a combination of pure shear and bending modes in a boundary layer on the left side.

The same boundary value problem is considered for a homogeneous substitution Cauchy medium endowed with the elastic properties of Table 1. The same clamping boundary conditions $U_1 = U_2 = 0$ are prescribed on the left side. The corresponding deformed shape is shown in Fig. 10(a). It shows that the Cauchy medium does not capture the bending mode of the composite structure and only provide the shearing mode. Quantitative comparison is possible in

TABLE 6: Higher order elastic properties of the overall micromorphic material for the unit cell of Figs. 1(a) and 1(b), no fluctuations

	Z_{1111} (MPa)	Z_{1122} (MPa)	Z_{2211} (MPa)	Z_{2222} (MPa)	Z_{1212} (MPa)	Z_{1221} (MPa)
(a)	2425	7001	5616	12064	16619	7166
(b)	–168	–4557	–101	–10717	–10492	–118
	η_{1111} (MPa)	η_{1122} (MPa)	η_{2211} (MPa)	η_{2222} (MPa)	η_{1212} (MPa)	η_{2112} (MPa)
(a)	2426	5616	7001	12064	16620	7165
(b)	–168	–101	–4557	–10716	–10490	–118
	ζ_{1111} (MPa)	ζ_{1122} (MPa)	ζ_{2222} (MPa)	ζ_{1212} (MPa)	ζ_{1221} (MPa)	ζ_{2121} (MPa)
(a)	92751	17508	57280	51441	19806	47275
(b)	848	98	24119	23964	47275	733
	A_{11} (MPa mm^2)	A_{22} (MPa mm^2)	A_{33} (MPa mm^2)	A_{12} (MPa mm^2)	A_{23} (MPa mm^2)	A_{13} (MPa mm^2)
(a)	2733	1051	1122	–1233	333	–469
(b)	28.0	52.7	623	–20.7	52.9	–285
	A_{66} (MPa mm^2)	A_{55} (MPa mm^2)	A_{44} (MPa mm^2)	A_{56} (MPa mm^2)	A_{45} (MPa mm^2)	A_{46} (MPa mm^2)
(a)	3892	865	1138	315	–541	–42.0
(b)	438	271	288	121	–258	–106

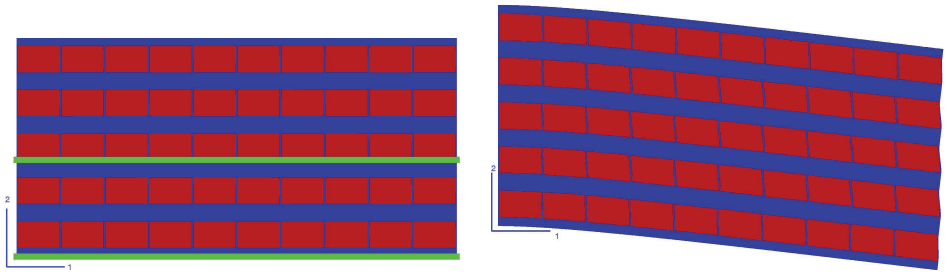

(a) (b)

FIG. 9: (a) Reference composite structure made of 10×5 cells and **(b)** reference deformed shape of the structure. Two horizontal lines are shown on the structure for post-processing purposes.

Fig. 11(a), where the displacement profile $U_2(x_1)$ is given along the horizontal line close to the mid-section of the structure, as drawn in Fig. 9. The bending induced by clamping is clearly visible on the reference curve and is absent from the Cauchy prediction. This fact was already noticed for laminates in Bacigalupo and Gambarotta (2010) and Forest and Sab (1998).

5.2 Computation with Three Different Generalized Homogeneous Substitution Media

The Cosserat and couple-stress media possess a bending stiffness that can improve the homogeneous description of the composite structure. The boundary value problem is again considered for such a Cosserat substitution medium endowed with the properties of Tables 2 and 3. Additional boundary conditions are necessary for such an enhanced continuum. Clamping is accounted for by the condition $\Phi_3 = 0$ on the left side of the structure, as is done in similar composite beam and plate problems. Figure 11(a) gives the displacement along the mid-line predicted by the Cosserat

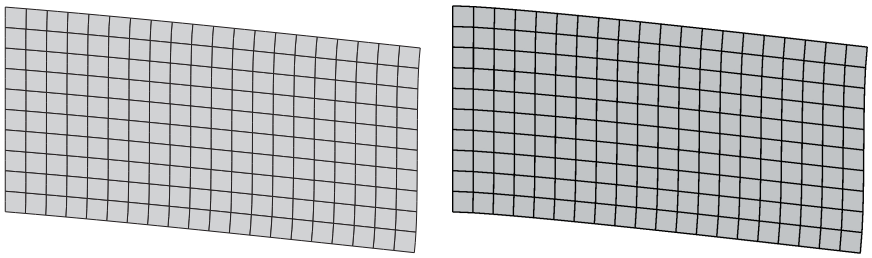

(a) (b)

FIG. 10: Deformed state of the structure made of a homogeneous substitution medium and subjected to the same displacement boundary conditions as in Fig. 9(b): **(a)** Cauchy substitution medium and **(b)** micromorphic substitution medium.

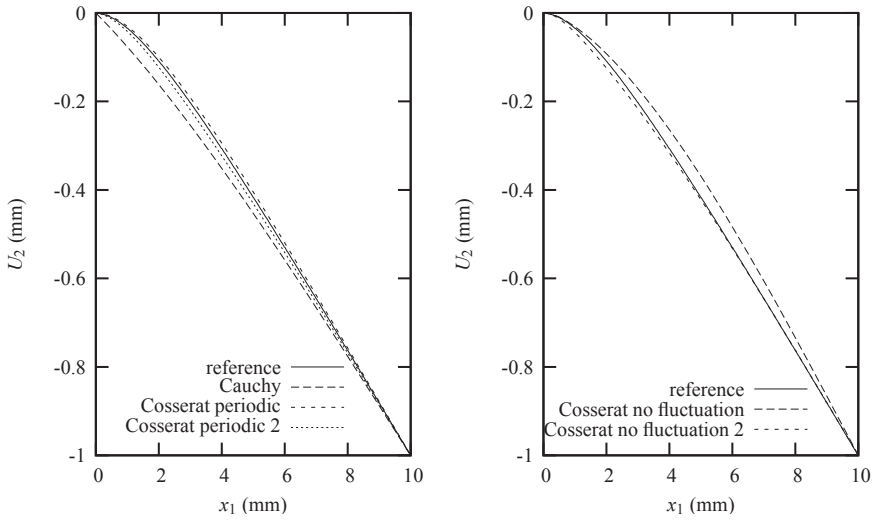

(a) (b)

FIG. 11: Vertical displacement component U_2 along the mid-line visible in Fig. 9 as computed for the reference structure and three different substitution media: **(a)** Cauchy continuum and Cosserat models with the coefficients of Table 2 (periodic fluctuation) for the two unit cells of Figs. 1(a) and 1(b) (labeled 2), **(b)** Cosserat model for a vanishing fluctuation and both unit cells.

continuum using the effective moduli derived from periodic boundary conditions on the two unit cells of Fig. 1. The predictions are very close to the reference result. The moduli based on the unit cell containing a hard cross deliver a slightly too soft response, whereas the moduli based on the unit cell of Fig. 1(a) are slightly too stiff. The predictions incorporating the effect of a periodic fluctuation are however better than the response of a Cosserat continuum endowed with moduli obtained without considering any fluctuation at the boundary of the unit cell. This is shown in Fig. 11(b). Note the compensating effect of "stiff" boundary conditions and "soft" unit cell, which eventually provides a good estimate. Almost perfect agreement between reference and homogeneous substitution media is obtained when the converged bending moduli are used, according to Table 2.

When the structure is made of a homogeneous second gradient medium endowed with the properties of Table 5, the deformed state of Fig. 10(a) and quantitative comparison in Fig. 12(a) show that no significant improvement is brought, probably due to the fact that we use moduli determined for a vanishing fluctuation. Converged moduli could not be determined because of zero–energy modes associated with some coefficient of the polynomial. A more spe-

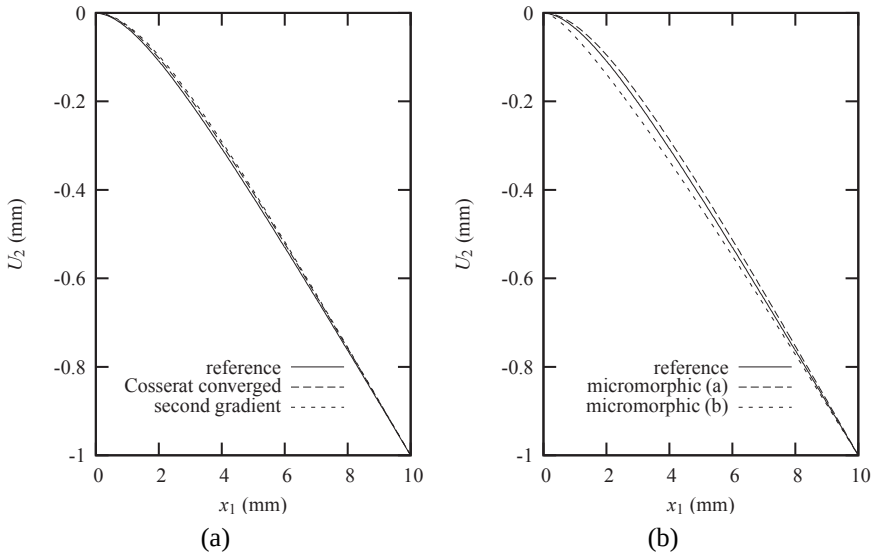

FIG. 12: Vertical displacement component U_2 along the mid-line visible in Fig. 9 as computed for the reference structure and three different substitution media: **(a)** Cosserat (converged bending moduli and periodic shear moduli) and second gradient models with the coefficients of Tables 2 and 5 for the unit cell of Fig. 1(a), and **(b)** micromorphic model with the two sets of coefficients of Table 6 corresponding to the unit cells of Figs. 1(a) and 1(b).

cific strategy should be developed to identify the relevant converged moduli. Also, the result obtained with the second gradient model shows that our example is not discriminant for selecting the best-suited generalized homogeneous substitution medium. More elaborate boundary value problems should be considered. The simulation for second gradient elasticity is made by means of a micromorphic formulation for which penalty terms ensure that the microdeformation coincide with the gradient of the displacement field. Clamping was imposed through the prescription of vanishing microdeformation on the left side. Note that the choice of the additional boundary conditions on the left side is quite heuristic, as it is the case in most beam and plate models.

The same simulation has been performed with the homogeneous micromorphic medium using the effective moduli of Table 6. The prediction of the deflection is also given in Fig. 12(b). It is in rather good agreement with the reference computation. The two considered unit cells deliver a slightly harder and softer response than the reference one.

The somewhat less good prediction of the micromorphic model compared to the Cosserat predictions of Figs. 11(a) and 12(b) may be due to the fact that the fluctuation was not considered in the identification.

An exact fit would be possible by significantly increasing the bending moduli of the Cosserat and second gradient moduli, but this is not done here because this would not correspond to a homogenization prediction. The better prediction of the micromorphic model is probably not due to the real need for a full micromorphic medium, because the Cosserat approach could be successful with different values of the effective moduli, but rather to the specific identification method for effective moduli.

It is remarkable that significantly different values of higher order moduli can lead to very close results. The response is to a certain extent not so sensitive to variations of higher order moduli. It means that the order of magnitude only of the bending moduli is essential to capture the bending effect in the proposed example. More discriminating tests are needed in future validations.

6. CONCLUSIONS

Cosserat, second gradient and micromorphic overall properties have been determined for a given highly contrasted two-phase elastic composite. The attention has been focused on the impact of the choice of the fluctuation displace-

ment on the derived effective higher order properties. Three possibilities were investigated: vanishing, periodic, or converged fluctuation field. The periodic and vanishing fluctuation deliver very close bending moduli, whereas the converged bending moduli are smaller. This shows that the application of non-homogeneous conditions at the boundary of the unit cell induce significant boundary layer effects even if periodicity is assumed. In contrast, when the curvature is applied remotely, we have found a converged curved state of a central unit cell embedded in a collection of N×N cells. In this way, we have defined a representative volume element size, here of about 9×9 cells, for which an exact fluctuation field was determined. This convergence analysis was also performed for the six coefficients of the quadratic polynomial. Because of the specific laminate microstructure, some loading conditions were found to correspond to zero–energy modes when applied sufficiently far from the boundaries. This fact has also been recognized by Bacigalupo and Gambarotta (2010) based on a different choice of the fluctuation displacement condition. These vanishing energy modes prevented us from determining a full matrix of higher moduli associated with the converged state.

A crucial point in the discussion is that, for the various considered fluctuation conditions, the average second gradient does not coincide with the coefficient D_{ijk} of the quadratic potential. That is why the post-processing formula (7), applicable to second gradient and micromorphic overall media, was put forward. On the basis of this expression, overall second gradient moduli were determined for a single unit cell with vanishing fluctuation. Additional work is needed to find out the moduli in the converged state at RVE size. An approximate scheme, taken from Jänicke (2010) and Jänicke et al. (2009), was then used for the determination of all micromorphic moduli, that amounts to assuming that K_{ijk} coincides with the coefficient of the polynomial.

The periodic fluctuation assumption was found to be rather bad-suited for third-order polynomials required in the Cosserat analysis. Indeed, the found Cosserat moduli associated with the skew-symmetric part of the stress, strongly differ whether the fluctuation is assumed to vanish or to be periodic. Also, in the micromorphic scheme, a special choice of the third-order polynomial was necessary in Jänicke (2010) to provide more satisfying effective moduli with regard to the validation problem. In fact, a precise selection of appropriate coefficients in the polynomials of orders larger that 2 remains to be done. At least third- and fourth-order polynomial are required for the identification of the full 3D micromorphic substitution medium.

A dependence on the choice of the unit cell was found for all approaches regarding the higher order moduli, the cross unit cell delivering the softest ones. The reference problem was satisfactorily described by all the presented substitution media. Improvement of the prediction was obtained when the moduli were obtained by taking the fluctuation conditions at the boundary. The test was not discriminating enough to conclude on the better quality of moduli based on converged fluctuation fields. Remarkably, even though some higher order moduli can be strongly different from one scheme to another, the predicted responses of the considered structural problem can remain very close.

The evaluation of the different methods suggests that the extended homogenization theory is still not in a fully satisfying state and raises several questions. Can we find an objective way to determine higher order moduli from computation on a single unit cell? The potential of the approach is high, as proved by the quality and reliability of the presented predictions. Accordingly, we propose a list of further steps in the development of a more systematic methodology for higher order homogenization:

1. Separate zero-energy modes in the polynomial development to derive overall moduli based on a converged fluctuation field
2. Find well-suited boundary conditions to derive these moduli from computations on a single unit cell
3. Get rid of the dependence on the choice of the unit cell or bring convincing arguments to select the best-suited one
4. Define complete boundary conditions to determine the overall properties of a full micromorphic medium (especially with respect to the non-symmetric parts of the micro-deformation gradient, which was not done in the present work)
5. Derive rules to determine the additional boundary conditions for the overall homogeneous substitution medium from the exact boundary conditions of the heterogeneous Cauchy structure

6. Design more discriminating examples to distinguish the best–suited substitution media

7. Extend the methodology to random media

Recent analytical results show that effective properties can indeed be determined independently of the the number of unit cells in a N×N unit cell (Bigoni and Drugan, 2007; Pham, 2010). However the dependence on the choice of the representative unit cell remains without solution. Are alternative approaches like multifield methods (Sansalone et al., 2005) and computational continua (Fish and Kuznetsov, 2010) more appropriate than the polynomial approach?

ACKNOWLEDGMENTS

Part of this work was carried out within the CPR project on Multifonctional Architectured Materials funded by CNRS, Arcelor–Mittal and EDF. This support is gratefully acknowledged.

REFERENCES

Auffray, N., Bouchet, R., and Bréchet, Y., Derivation of anisotropic matrix for bi–dimensional strain–gradient elasticity behavior, *Int. J. Solids Struct.*, vol. **46**, pp. 440–454, 2009.

Auffray, N., Bouchet, R., and Bréchet, Y., Strain gradient elastic homogenization of bidimensional cellular media, *Int. J. Solids Struct.*, vol. **47**, pp. 1698–1710, 2010.

Bacigalupo, A. and Gambarotta, L., Second-order computational homogenization of heterogeneous materials with periodic microstructure, *ZAMM*, vol. **90**, pp. 796–811, 2010.

Bigoni, D. and Drugan, W. J., Analytical derivation of Cosserat moduli via homogenization of heterogeneous elastic materials, *J. Appl. Mech.*, vol. **74**, pp. 741–753, 2007.

Boutin, C., Microstructural effects in elastic composites, *Int. J. Solids Struct.*, vol. **33**, pp. 1023–1051, 1996.

Bouyge, F., Jasiuk, I., and Ostoja-Starzewski, M., A micromechanically based couple-stress model of an elastic two-phase composite, *Int. J. Solids Struct.*, vol. **38**, pp. 1721–1735, 2001.

De Bellis, M. L. and Addessi, D., A Cosserat based multi–scale model for masonry structures, *Int. J. Multiscale Eng.*, vol. **9**, pp. 543–563, 2011.

Dell'Isola, F., Rosa, L., and Woźniak, C., A micro-structured continuum modelling compacting fluid-saturated grounds: The effects of pore-size scale parameter, *Acta Mech.*, vol. **127**, pp. 165–182, 1998.

Dillard, T., Forest, S., and Ienny, P., Micromorphic continuum modelling of the deformation and fracture behaviour of nickel foams, *Eur. J. Mech. A*, vol. **25**, pp. 526–549, 2006.

Ebinger, T., Steeb, H., and Diebels, S., Modeling macroscopic extended continua with the aid of numerical homogenization schemes, *Comput. Mater. Sci.*, vol. **32**, pp. 337–347, 2005.

Eringen, A. C. and Suhubi, E. S., Nonlinear theory of simple microelastic solids, *Int. J. Eng. Sci.*, vol. **2**, pp. 189–203, 389–404, 1964.

Feyel, F., A multilevel finite element method (FE2) to describe the response of highly non-linear structures using generalized continua, *Comput. Methods Appl. Mech. Eng.*, vol. **192**, pp. 3233–3244, 2003.

Fish, J. and Kuznetsov, S., Computational continua, *Int. J. Numer. Methods Eng.*, vol. **84**, pp. 774–802, 2010.

Forest, S., Mechanics of generalized continua: Construction by homogenization, *J. Phys. IV*, vol. **8**, pp. Pr4–39–48, 1998.

Forest, S., Aufbau und identifikation von stoffgleichungen für höhere kontinua mittels homogenisierungsmethoden, *Tech. Mech.*, vol. **19**, no. 4, pp. 297–306, 1999.

Forest, S., Homogenization methods and the mechanics of generalized continua—Part 2, *Theor. Appl. Mech.*, vol. **28–29**, pp. 113–143, 2002.

Forest, S., The micromorphic approach for gradient elasticity, viscoplasticity and damage, *ASCE J. Eng. Mech.*, vol. **135**, pp. 117–131, 2009.

Forest, S. and Sab, K., Cosserat overall modeling of heterogeneous materials, *Mech. Res. Commun.*, vol. **25**, no. 4, pp. 449–454, 1998.

Forest, S. and Trinh, D. K., Generalized continua and non–homogeneous boundary conditions in homogenization methods, *ZAMM*, vol. **91**, pp. 90–109, 2011.

Geers, M. G. D., Kouznetsova, V. G., and Brekelmans, W. A. M., Gradient–enhanced computational homogenization for the micro–macro scale transition, *J. Phys. IV*, vol. **11**, pp. Pr5–145–152, 2001.

Gologanu, M., Leblond, J. B., and Devaux, J., Continuum micromechanics, Recent extensions of Gurson's model for porous ductile metals, CISM Courses and Lectures no. 377, Springer-Verlag, Berlin, pp. 61–130, 1997.

Jänicke, R., Micromorphic media: Interpretation by homogenisation, PhD-thesis, Saarbrücker Reihe Materialwissenschaft und Werkstofftechnik, Band 21. Shaker Verlag, Aachen, http://scidok.sulb.uni-saarland.de/volltexte/2010/3209, 2010.

Jänicke, R. and Diebels, S., A numerical homogenisation strategy for micromorphic continua, *Nuovo Cimento Soc. Ital. Fis C-Geophys. Space Phys.*, vol. **32**, pp. 121–132, 2009.

Jänicke, R., Diebels, S., Sehlhorst, H.-G., and Düster, A., Two–scale modelling of micromorphic continua, *Continuum Mech. Thermodyn.*, vol. **21**, pp. 297–315, 2009.

Kaczmarczyk, L., Pearce, C. J., and Bicanic, N., Scale transition and enforcement of RVE boundary conditions in second-order computational homogenization, *Int. J. Numer. Methods Eng.*, vol. **74**, pp. 506–522, 2008.

Kanit, T., Forest, S., Galliet, I., Mounoury, V., and Jeulin, D., Determination of the size of the representative volume element for random composites: Statistical and numerical approach, *Int. J. Solids Struct.*, vol. **40**, pp. 3647–3679, 2003.

Kouznetsova, V., Geers, M. G. C., and Brekelmans, W. A. M., Size of a RVE in a second order computational homozenization framework, *Int. J. Multiscale Comput. Eng.*, vol. **2**, pp. 575–598, 2004a.

Kouznetsova, V. G., Geers, M. G. D., and Brekelmans, W. A. M., Multi-scale second-order computational homogenization of multi-phase materials: A nested finite element solution strategy, *Comput. Methods Appl. Mech. Eng.*, vol. **193**, pp. 5525–5550, 2004b.

Larsson, R. and Diebels, S., A second-order homogenization procedure for multi-scale analysis based on micropolar kinematics, *Int. J. Num. Methods Eng.*, vol. **69**, pp. 2485–2512, 2007.

Masiani, R. and Trovalusci, P., Cosserat and Cauchy materials as continuum models of brick masonry, *Meccanica*, vol. **31**, pp. 421–432, 1996.

Mindlin, R. D., Micro–structure in linear elasticity, *Arch. Rat. Mech. Anal.*, vol. **16**, pp. 51–78, 1964.

Mindlin, R. D. and Eshel, N. N., On first strain gradient theories in linear elasticity, *Int. J. Solids Struct.*, vol. **4**, pp. 109–124, 1968.

Mühlich, U., Zybell, L., and Kuna, M., Micromechanical modelling of size effects in failure of porous elastic solids using first oder plane strain gradient eslaticity, *Comput. Mater. Sci.*, vol. **46**, pp. 647–653, 2009.

Ostoja-Starzewski, M., Boccara, S. D., and Jasiuk, I., Couple-stress moduli and characteristic length of two-phase composite, *Mech. Res. Commun.*, vol. **26**, pp. 387–396, 1999.

Pham, T. T. T., Un modèle d'endommagement à gradient de déformation à partir de la méthode d'homogénéisation pour les matériaux fragiles, Phd thesis, Université Paris XIII, 2010.

Sansalone, V., Trovalusci, P., and Cleri, F., Multiscale modeling of composite materials by a multifield finite element approach, *Int. J. Multiscale Comput. Eng.*, vol. **3**, pp. 463–480, 2005.

Tekoglu, C. and Onck, P. R., Size effects in two-dimensional Voronoi foams: A comparison between generalized continua and discrete models, *J. Mech. Phys. Solids*, vol. **56**, pp. 3541–3564, 2008.

Triantafyllidis, N. and Bardenhagen, S., The influence of scale size on the stability of periodic solids and the role of associated higher order gradient continuum models, *J. Mech. Phys. Solids*, vol. **44**, pp. 1891–1928, 1996.

Trovalusci, P. and Masiani, R., Non-linear micropolar and classical continua for anisotropic discontinuous materials, *Int. J. Solids Struct.*, vol. **40**, pp. 1281–1297, 2003.

Yuan, X., Tomita, Y., and Andou, T., A micromechanical approach of nonlocal modeling for media with periodic microstructures, *Mech. Res. Commun.*, vol. **35**, pp. 126–133, 2008.